The Intrinsic Structural Resistance of a Grain Boundary to Transverse Ionic Conduction

Annalena R. Genreith-Schriever,* Jana P. Parras, Henrik J. Heelweg, and Roger A. De Souza[a]

Ion transport across grain boundaries in diverse polycrystalline ionic conductors is often found to be hindered. Such behaviour is commonly attributed to the presence of a highly resistive second phase or to the presence of space-charge zones, in which mobile charge carriers are strongly depleted. One other possible cause – the severe perturbation of the crystal structure within the grain-boundary core – is widely ignored. Employing molecular dynamics (MD) simulations of the model Σ5(310) [001] grain boundary in fluorite-structured CeO_2, we demonstrate an approach to extract the intrinsic structural resistance of a grain boundary (to ionic transport across it), and we determine this excess resistance as a function of temperature. Compared with space-charge resistances predicted for a dilute solution of charge carriers the structural resistance of this interface is orders of magnitude smaller at temperatures below $T \approx 1000$ K but at $T > 1200$ K it is no longer negligible.

The arrangement of ions in various crystal structures allows particular ions to migrate through the structures at astonishing rates. Characteristic examples are garnet-type $Li_7La_3Zr_2O_{12}$ for Li^+,[1–3] fluorite-type CeO_2 for O^{2-},[4–8] and perovskite-type $BaZrO_3$ for H^+.[9–11] These and similar materials are generally characterised by high-symmetry structures comprising a continuous network of migration paths with low-energy barriers linking sites of comparable energy.[12–16] The application of such materials in solid-state electrochemical devices (*e.g.* in batteries and fuel cells) is not in the form of single crystals, however; rather it is in the form of polycrystals, whose grain boundaries are found to diminish the overall rate of ion transport.[17–24] The high resistance to ion transport presented by the grain boundaries is often attributed to highly resistive second phases or to space-charge layers depleted of the mobile charge carriers.[25–31] A third possibility is rarely considered: the resistance arising from the perturbed crystal structure. High-conductivity crystal structures already offer ideal, or very close to ideal, conditions for ion transport, and consequently, any perturbation of that crystal structure is expected to result in diminished transport rates.[32,33] Specifically, the ion arrangements at interfaces differ considerably from those in the bulk, in terms of symmetry and altered inter-ionic distances. These differences are expected to result in a more complex energy hypersurface with increased activation barriers of migration. As a consequence, grain boundaries in the best ionic conductors will exhibit an intrinsic structural resistance. The unanswered question at this time is how large this resistance is.

Increased structural resistance is invoked on rare occasion in the literature.[34–36] In some cases, there are, however, problems with the analyses, mainly because there is no approach available that selectively probes the intrinsic structural grain-boundary resistance. Experimental grain-boundary resistances reported so far may conceivably contain contributions both from space-charge effects and from the structural perturbation. Kim and Lubomirsky[35,37] suggested an elegant method to differentiate between space-charge related resistances and other resistances, such as those arising from current constriction caused by secondary phases or from structural perturbation. In their method, the grain-boundary electrostatic potential obtained by analysing the ratio of grain-boundary to bulk resistances (an analysis that is based on the explicit premise of the structural and other resistances being negligible) is compared with the potential obtained by analysing the power-law dependence of the current voltage behaviour at boundaries. Unfortunately, this approach does not allow the intrinsic structural resistance to be separated from other non-space-charge related resistances. Furthermore, in cases where a non-space-charge resistance has been conjectured, the systems under consideration were all concentrated solid solutions, but were analysed in terms of dilute-solution theories. The examination of a far more dilute solution does not yield a difference between the two.[38] Any difference extracted from a comparison of the power-law behaviour and the resistance ratio could therefore arise from treating a concentrated solid solution with dilute-solution models.[39] The validity of the authors' conclusions about non-space-charge related contributions is, therefore, doubtful.

Computational investigations provide, in theory, a superior approach as they could generally differentiate between space-charge and structural resistances. They could hence provide data that cannot, at least at present, be obtained experimentally. Molecular dynamics (MD) studies of ion transport in polycrystalline Li-ion and Na-ion electrolytes suffer, however, from monitoring the mean-square-displacements (MSD) of ions.[40–42] Consequently, the transport coefficient obtained is the tracer diffusion coefficient D^*. In order to convert D^* into a

[a] Dr. A. R. Genreith-Schriever, J. P. Parras, H. J. Heelweg, Prof. Dr. R. A. De Souza
Institute of Physical Chemistry
RWTH Aachen University
Landoltweg 2, 52056 Aachen, Germany
E-mail: Annalena.Genreith.Schriever@rwth-aachen.de

conductivity σ (with the Nernst-Einstein equation), one needs for a dilute solution of charge carriers the tracer correlation coefficient f^*. For ion transport in a bulk phase, f^* is a constant of order unity that depends on the migration mechanism (vacancy, interstitial, interstitialcy) and the symmetry of the sublattice on which the ions are moving.[43] For ion transport at a grain boundary, f^* will necessarily differ from the bulk value, as the grain boundary does not possess the same symmetry as the bulk; and conceivably it may depend strongly on temperature and take values orders of magnitude lower than unity. The conversion from D^* to σ for grain boundaries is, therefore, far from trivial, even for dilute solutions. The second problem from which simulation studies suffer is that diffusivities are resolved locally based on the MSDs of ions in a specific region of the supercell.[40,41] While a local resolution is in principle ideal for accurately extracting the properties of a grain boundary, the MSD analysis is restricted by the displacements being defined relative to the starting positions of the ions (at the beginning of the simulation). After a simulation run of several nanoseconds, as performed in the reported studies,[40,41] the ions that were originally in the grain-boundary region of the supercell are very likely to also have spent certain amounts of time in the bulk regions of the supercell. Considering the derived resistivities to be the resistivities solely of the grain boundaries is, therefore, problematic. A procedure is thus lacking that permits the intrinsic structural resistivity of a grain boundary to be extracted, free from contributions of the surrounding bulk regions and without space-charge effects.

In this Communication, we propose a method to directly determine the intrinsic structural resistance of a grain boundary in an ionic conductor. Our approach is based on large-scale classical MD simulations under applied electric fields. We obtain the intrinsic resistance, as an excess quantity, as a function of temperature for a symmetric tilt boundary, the Σ5(310)[001] grain boundary, in oxygen-deficient ceria. And having obtained the intrinsic structural resistance, we compare it with the excess resistance arising from space-charge layers at this boundary. The selected interface and material, it is emphasised, both offer prototypic conditions: ceria (CeO_2) is a model material for fluorite-structured energy materials[44] for which oxide-ion transport is well characterised and understood, both computationally[45–53] and experimentally.[5–7,54–58] The Σ5(310)[001] grain boundary is a model grain boundary for several reasons: it was experimentally shown to be one of the prevalent boundaries in fluorite-structured oxides;[59] its structure has been analysed experimentally;[60] and its small repeat unit makes it a good candidate for simulation studies.[61–65]

The energy-optimised simulation cell with two anti-parallel Σ5(310)[001] grain boundaries is shown in Figure 1. The atomistic structure of the grain boundary is in good agreement with previous experimental and computational studies.[60–62,66–71] Characteristic excess quantities of the boundary, the excess grain-boundary energy $\Delta E_{gb} = 2.85\ J\,m^{-2}$ and excess volume $\Delta V_{gb} = 0.90\ Å^3\,Å^{-2}$, also agree well with literature.

To obtain oxide-ion mobilities we introduced oxygen vacancies into the simulation cell (site fraction of vacancies $n_v = 0.10\,\%$) and subjected the cell to electric fields along the x direction of the simulation cell – perpendicular to the grain boundary – by applying an additional force $F = qE$ to each ion (where q is the charge of the ion). For reference purposes, we also calculated the bulk mobility as a function of field strength in supercells of $Ce_{7680}O_{15345}$, *i.e.* with the same site fraction of oxygen vacancies but without grain boundaries.

In Figure 2 we plot the oxide-ion mobility obtained from the MD simulations as a function of field strength for various temperatures. For the single-crystal cell [Figure 2(a)], u is independent of E at small values of E but increases strongly at large values. This behaviour is in good agreement with the standard model of field-enhanced ion transport dating back to Verwey,[73] Mott and Gurney,[74] and Frenkel.[25] Quantitatively, however, this standard treatment overestimates the mobility enhancement at high fields.[53] We previously suggested[53] a

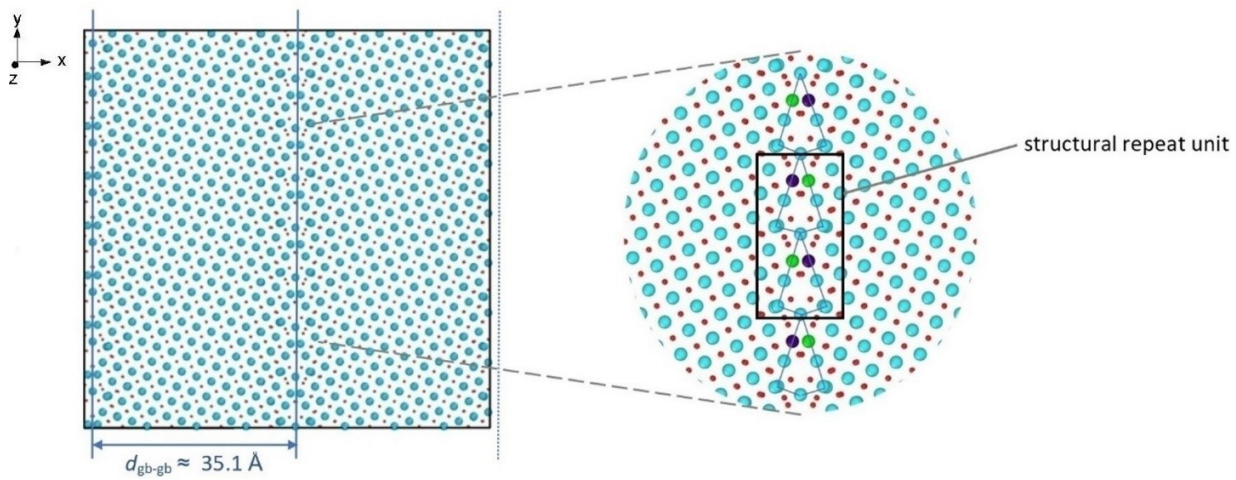

Figure 1. Supercell containing two anti-parallel Σ5(310)[001] grain boundaries, one at the centre of the cell and one half at each side (indicated with blue lines), as obtained from MD simulations in combination with rigid-body translations[72] and final energy optimisations, viewed along the [001] axis (corresponding to the z direction of the simulation cell); the blue spheres denote cerium ions and the red spheres, oxide ions. In the closeup, the characteristic structural unit is sketched (solid line) and alternating positions of two cerium ions are indicated in green and purple.

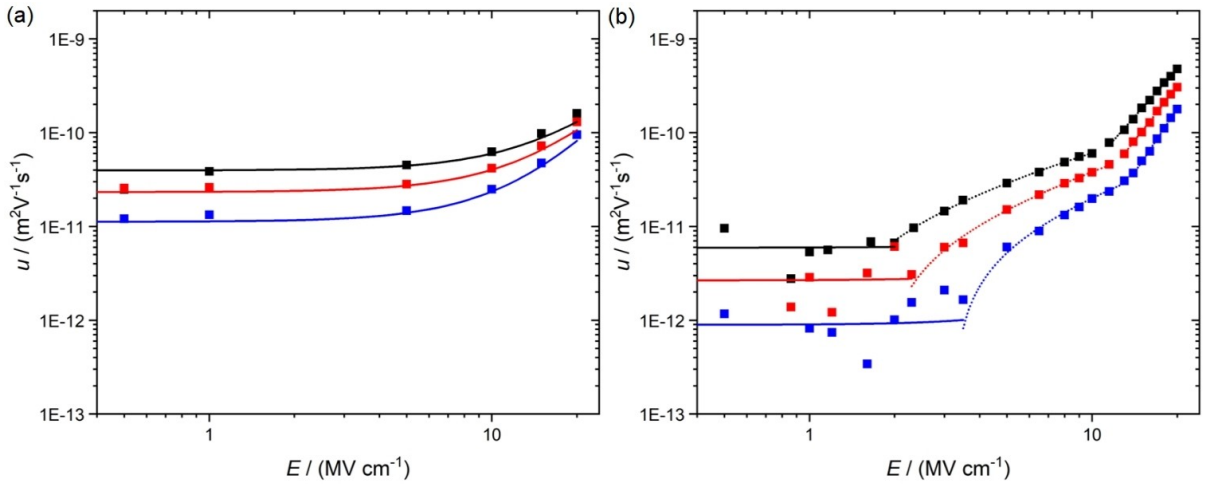

Figure 2. Mobility of oxide ions u as a function of field strength E at $T/K = 1200$ (blue data points), 1400 (red data points), and 1600 (black data points), a) for the single-crystal supercell; b) for the supercell with two grain boundaries. The solid lines show the predictions of our previously proposed model[53] assuming an activation barrier of migration of $\Delta H_{mig} = 0.64$ eV in the bulk and $\Delta H_{mig} = 0.9$ eV in the simulation cell with grain boundaries.

superior expression for $u(E,T)$, which, as one can see in Figure 2(a), describes the simulation data extremely well. The activation enthalpy of oxide-ion migration used to describe the data is $\Delta H_{mig} = 0.64$ eV.

In comparison, the data obtained for the bicrystal supercell [Figure 2(b)] show complex behaviour with three apparent regimes. At small E (< 2 MV cm^{-1}), u is evidently independent of field strength. The scatter seen in the data is caused by the finite number of ion jumps occurring during the simulation runs. Ion drift requires ion jumps to take place, and as the jump process is a biased stochastic process, the exact number of jumps will show some natural variation. We can describe these data using our standard expression[53] with $\Delta H_{mig} = 0.9$ eV; this effectively assumes that the complex energy hypersurface at the boundaries can be approximated by a single increased activation barrier. Thus in the limit of low fields, the oxide-ion mobility is lower and the effective migration barrier is higher for the cell containing the grain boundaries. These boundaries clearly constitute a resistance to the drift of oxide ions through the cell.

At higher fields, $E > 2$ MV cm^{-1}, there are two field-dependent regimes: an intermediate-field regime extending up to *ca.* 10 MV cm^{-1}, and then a high-field regime. For the latter, u, surprisingly, is higher for the bicrystal cell than for the bulk cell. This complex behaviour could be caused by a simulation artefact. Increased energy dissipation at the boundaries could, for example, result in temperature gradients within the simulation cell, an effect that would make itself particularly evident at higher fields. Analysis of our simulations, however, indicated constant temperatures across the cell. Alternatively, the field could cause the boundary structure to change substantially,[75] and in this way, affect the migration barrier(s), but such substantial changes were not observed in our simulations. If the origin of the high-field behaviour lies in the system, then at higher fields the behaviour cannot be described with a single, increased activation barrier. Hence, we tentatively ascribe the behaviour to the multiplicity of inequivalent jump paths at the boundaries and corresponding activation barriers in the boundary region.[34,76] Empirically we found [see Figure 2(b)] that the two high-field regimes can be described with $u \propto \ln E$ and with $u \propto E^{3.3-4.5}$, respectively. These functional forms do not provide any immediate clues, however, as to the physical origins of the two regimes. A detailed examination of this issue is left for future study.

The final issue we examine is whether the intrinsic structural resistance needs to be taken into account when analysing experimental data or whether it can be neglected. To this end, we compare the intrinsic structural (^{is}) resistance of this $\Sigma 5(310)[001]$ boundary with the resistances that arise at this boundary from space-charge layers (^{scl}). In both cases, we consider the resistance as an excess quantity, ΔR_{gb}, and we restrict the considerations to the low-field regime.

Starting with the intrinsic structural case, we thus write the total electrical resistance of the cell containing two grain boundaries as the resistance of a hypothetical bulk supercell with identical dimensions plus the two excess grain-boundary resistances to account for the two grain boundaries in the simulation cell, $R_{cell} = R_b + 2\Delta R_{gb}^{is}$. Upon rearranging, normalising to the bulk resistance, and linking resistances via conductivities to mobilities, we obtain

$$\frac{\Delta R_{gb}^{is}}{R_b} = \frac{1}{2}\left(\frac{u_b}{u_{cell}} - 1\right) \quad (1)$$

where u_b and u_{cell} are the oxide-ion mobilities in the bulk and in the simulation cell with grain boundaries, respectively. The resistance ratio can thus be determined directly from the oxide-ion mobility in the bulk cell and in the supercell with grain boundaries (as long as the same material is investigated in the bulk and grain-boundary cells with identical charge-carrier concentrations, the model requires no material-specific input and can thus be transferred directly to other materials). Using

the analytical (low-field) descriptions[53] shown in Figure 2 (rather than the actual mobility data), we calculated $\Delta R^{is}_{gb}/R_b(T)$. Such results, we emphasise, correspond to a bulk phase with the length of the simulation supercell, l_{cell}. The values for a polycrystalline sample with a typical grain size of l_{gr} are a factor l_{cell}/l_{gr} smaller, and in Figure 3 we plot $\Delta R^{is}_{gb}/R_b(T)$ calculated for $l_{gr}=1$ μm and extrapolated to lower temperatures. The temperature dependence of the resistance ratio is fairly weak, with an effective activation energy of (0.9 eV–0.64 eV) = 0.26 eV.

In considering ΔR^{scl}_{gb}, we restricted the space-charge treatment to a dilute solution of oxygen vacancies, in order to make the results comparable to those obtained above for ΔR^{is}_{gb}. As specific charge-compensating defects we have taken acceptor-type cations with a single negative effective charge. The bulk electroneutrality condition is thus $n_a = 4n_v$. The general thermodynamic theory of space-charge formation[29,30,39,77,78] was used to calculate $\Delta R^{scl}_{gb}/R_b$ for the Σ5(310)[001] grain boundary in ceria. According to the theory, space-charge formation is driven by the non-zero Gibbs energies for point defects segregating from the bulk phase to the grain-boundary core. Atomistic calculations of this boundary[62,65] indicate that there are $N^c_v = 1.26\times10^{28}$ m^{-3} sites with a segregation energy of −1.1 eV for oxygen vacancies and $N^c_a = 2.81\times10^{27}$ m^{-3} sites with a segregation energy of −0.4 eV for the acceptors.

As expected,[29,39,77–79] the vacancy segregation energy is strongly negative and thus will dominate the overall behaviour. It forces (mobile) oxygen vacancies to segregate to the core from the bulk, charging the core positive and creating depletion space-charge zones. We consider three specific cases for the behaviour of the acceptor-dopant cations in the space-charge zones:[79] in the Mott-Schottky case, the dopant concentration is constant throughout the system owing to the dopant cations being immobile; in the Gouy-Chapman case, the cation dopants are mobile, and – reacting to the potential profile set up by the vacancies' redistribution – they develop equilibrium accumulation profiles; in the restricted equilibrium case, the dopant accumulation profile is frozen in from some critical temperature (T_{crit}) below which the dopant cations are insufficiently mobile to achieve electrochemical equilibrium. In all three cases, oxygen vacancies are mobile and achieve electrochemical equilibrium. Finite-element-method (FEM) calculations were used to obtain $\Delta R^{scl}_{gb}/R_b(T)$ considering, with good reason, that only the oxygen vacancies contribute to the measured resistances.[79]

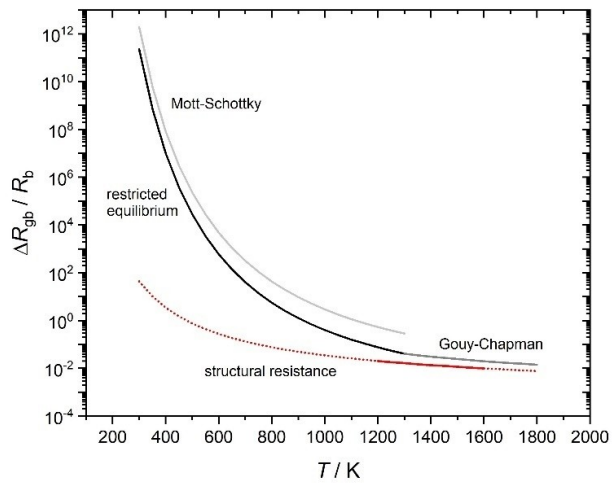

Figure 3. Excess resistance of a Σ5(310)[001] grain boundary in acceptor-doped CeO_2 relative to the bulk resistance ($l_{gr}=1$ μm) as a function of temperature: Space-charge resistances predicted for the Mott-Schottky case (light grey), Gouy-Chapman case (dark grey), and restricted-equilibrium case (black); the intrinsic structural resistance (red).

The space-charge resistances shown in Figure 3 refer to the following heating-cooling thought experiment performed on a grain of length $l_{gr}=1$ μm: We assume arbitrarily that the Mott-Schottky case is valid from room temperature up to $T_{crit}=1300$ K, beyond which the acceptors are considered to be sufficiently mobile that the Gouy-Chapman case results. On cooling, the acceptor accumulation profile is frozen in below $T_{crit}=1300$ K (restricted equilibrium). Comparing the two sets of data for this boundary, we find for a dilute solution of charge carriers that the structural resistance is of the same order of magnitude as, though lower than, the space-charge resistance at $T>1200$ K. At lower temperatures, however, the structural resistance becomes negligible.

Since our emphasis in this Communication has been on presenting the method, we end by noting that the generality of the results shown in Figure 3 remains to be clarified of course.

First, it needs to be determined if $\Delta R^{scl}_{gb} \gg \Delta R^{is}_{gb}$ holds for the majority of grain boundaries interacting with a dilute solution of point defects at the temperatures of interest. The two excess resistances will not necessarily vary in the same manner with the grain-boundary's degree of structural perturbation, since different parameters are important in the two cases.

While ΔR^{scl}_{gb} is governed by the thermodynamic driving energies, ΔR^{is}_{gb} will depend strongly on the modified kinetic barriers. In this sense, it is worth noting that Tschoepe *et al.* derived a segregation energy for oxygen vacancies for ceria polycrystals of −2.2 eV,[80] indicating a far stronger driving energy than the one used here. Second, the extension to concentrated solid solutions needs to be made. A framework already exists to calculate ΔR^{scl}_{gb} taking into account defect-defect interactions,[31,39] but the calculation of ΔR^{is}_{gb} will be far more complicated on account of the modified composition of the grain boundaries.

In summary, we have proposed a new approach to determine the structural resistance of a grain boundary, separate from other effects, namely large-scale MD simulations. We applied our approach to determine the excess structural resistance of the Σ5(310)[001] tilt boundary in ceria as a function of temperature. Three observations are of particular interest.

First, at low fields, the oxide-ion mobility in the simulation cell with grain boundaries is lower than in the bulk. The mobility can be described with an effective migration barrier of $\Delta H_{mig}=0.9$ eV, which is higher than the bulk value of 0.64 eV. This illustrates the intrinsic structural resistance of the grain boundary.

Second, at large fields the behaviour can no longer be accounted for by a single effective barrier. Current analytical models will need to take into account the more complex energy hypersurface at the boundary.

Third, at temperatures $T > 1200$ K, the intrinsic structural resistance is comparable to the space-charge resistance calculated for typical acceptor scenarios. This challenges the premise of most current space-charge studies – that the structural resistance can be neglected under all conditions.

Computational Methods

The simulations were based on the Born model of ionic solids,[81] treating the ions as classical particles that interact through long-range electrostatic interactions and parametrised Buckingham pair potentials.[82] This description has been successfully applied to simulating CeO_2 in diverse cases.[50,82–85] All simulations were performed with the LAMMPS code.[86] Optimisations were performed at constant pressure $p = 0$, while MD simulations were performed for the isothermal isobaric ensemble *NpT* over simulation times of 3 ns.

Using the gosam software,[87] we generated an initial grain-boundary supercell with 23,040 ions containing two anti-parallel Σ5(310)[001] grain boundaries. (This involved the rotation of two fluorite-structured ($Fm\bar{3}m$) ceria grains around the [001] axis by $\theta = 36.9^\circ$, so that their (310) planes coincided.) Subsequently, we performed three-dimensional rigid-body translations of the two grains,[88] and for all configurations we then carried out annealing at high temperatures in MD simulations to obtain the lowest energy grain-boundary structure.

The final supercell had dimensions of *ca.* 65.3 Å × 68.7 Å × 70.3 Å; the two anti-parallel boundaries are thus separated by a distance of $d_{gb-gb} = 35.1$ Å (see Figure 1).

Oxygen vacancies were introduced into the supercell by removing oxide ions at random. In order to compensate the charge of the vacancies, we slightly decreased the charge of all cerium cations. The site fraction of oxygen vacancies was set at $n_v = 0.10\,\%$, *i.e.* within the dilute regime.[39] In this way, vacancies are unlikely to site block the migration of other vacancies and the change in the charge of the cations is kept small (*ca.* $4 \times 10^{-3}\ e$). By changing the charge of all the cations rather than substituting specific Ce cations with trivalent dopant cations, we avoid introducing complexities into the transport behaviour due to vacancy-dopant interactions.[45–49]

At temperatures $1200 < T/\mathrm{K} < 1600$ and field strengths $10^{-0.4} < E/\mathrm{MV\,cm^{-1}} < 10^{1.3}$ we monitored $< |x_i| >$, the mean displacement of the oxide ions in the *x* direction (averaged over all oxide ions). The system was equilibrated during a 50 ps run (at the end of which the system's energy only showed fluctuations around a certain value), followed by a simulation run of 3 ns. $< |x_i| >$ was found to show a linear increase with time *t* at each temperature. The drift velocity of the oxide ions was determined from $v_d = d < |x_i| > /dt$, from which the ion mobility was then obtained as $u = v_d/E$.

Acknowledgements

We gratefully acknowledge financial support from the German Science Foundation (DFG) within the framework of the collaborative research centre "Nanoswitches" (SFB 917). Simulations were performed with computing resources granted by RWTH Aachen University under project rwth0189 and by JARA-HPC from RWTH Aachen University under project jara0100. Open access funding enabled and organised by Projekt DEAL.

Conflict of Interest

The authors declare no conflict of interest.

Keywords: computational chemistry · electrical resistance · grain boundaries · molecular dynamics

[1] R. Murugan, V. Thangadurai, W. Weppner, *Angew. Chem. Int. Ed.* **2007**, *46*, 7778–7781; *Angew. Chem.* **2007**, *119*, 7925–7928.
[2] C. A. Geiger, E. Alekseev, B. Lazic, M. Fisch, T. Armbruster, R. Langner, M. Fechtelkord, N. Kim, T. Pettke, W. Weppner, *Inorg. Chem.* **2011**, *50*, 1089–1097.
[3] V. Thangadurai, S. Narayanan, D. Pinzaru , *Chem. Soc. Rev.* **2014**, *43*, 4714–4727.
[4] H. L. Tuller, A. S. Nowick, *J. Electrochem. Soc.* **1975**, *122*, 255.
[5] H. Inaba, H. Tagawa, *Solid State Ionics* **1996**, *83*, 1–16.
[6] B. Steele, *Solid State Ionics* **2000**, *129*, 95–110.
[7] M. Mogensen, N. M. Sammes, G. A. Tompsett, *Solid State Ionics* **2000**, *129*, 63–94.
[8] A. Orera, P. R. Slater, *Chem. Mater.* **2010**, *22*, 675–690.
[9] H. Iwahara, T. Yajima, T. Hibino, K. Ozaki, H. Suzuki, *Solid State Ionics* **1993**, *61*, 65–69.
[10] T. Norby, *Solid State Ionics* **1999**, *125*, 1–11.
[11] K. D. Kreuer, *Annu. Rev. Mater. Res.* **2003**, *33*, 333–359.
[12] W. van Gool, *Annu. Rev. Mater. Sci.* **1974**, *4*, 311–335.
[13] R. A. Huggins in *Very Rapid Ionic Transport in Solids* (Eds.: A. S. Nowick, J. J. Burton), Academic Press, NY, USA, **1975**, pp. 445-486.
[14] H. Schulz, *Annu. Rev. Mater. Sci.* **1982**, *12*, 351–376.
[15] J. B. Goodenough, *Proc. R. Soc. A* **1984**, *393*, 215–234.
[16] S. Hull, *Rep. Prog. Phys.* **2004**, *67*, 1233–1314.
[17] A. Tschoepe, R. Birringer, *J. Electroceram.* **2001**, *7*, 169–177.
[18] A. Tschoepe, E. Sommer, R. Birringer, *Solid State Ionics* **2001**, *139*, 255–265.
[19] A. Tschoepe, *Solid State Ionics* **2001**, *139*, 267–280.
[20] X. Guo, W. Sigle, J. Maier, *J. Am. Ceram. Soc.* **2003**, *86*, 77–87.
[21] X. Guo, *Scr. Mater.* **2011**, *65*, 96–101.
[22] D. Y. Wang, A. S. Nowick, *J. Solid State Chem.* **1980**, *35*, 325–333.
[23] M. C. Gobel, G. Gregori, J. Maier, *Phys. Chem. Chem. Phys.* **2014**, *16*, 10175–10186.
[24] S. Kim, P. Jain, H. J. Avila-Paredes, A. Thron, K. van Benthem, S. Sen, *J. Mater. Chem.* **2010**, *20*, 3855–3858.
[25] J. Frenkel, *Kinetic Theory of Liquids*, Oxford University Press, New York, **1946**.
[26] K. L. Kliewer, J. S. Koehler, *Phys. Rev.* **1965**, *140*, 1226–1240.
[27] K. Lehovec, *Phys. Rev.* **1953**, *90*, 350.
[28] J. Jamnik, J. Maier, S. Pejovnik, *Solid State Ionics* **1995**, *75*, 51–58.
[29] R. A. De Souza, *Phys. Chem. Chem. Phys.* **2009**, *11*, 9939–69.
[30] D. Bingham, P. W. Tasker, A. N. Cormack, *Philos. Mag. A* **1989**, *60*, 1–14.
[31] D. S. Mebane, R. A. De Souza, *Energy Environ. Sci.* **2015**, *8*, 2935–2940.
[32] V. Metlenko, A. H. H. Ramadan, F. Gunkel, H. Du, H. Schraknepper, S. Hoffmann-Eifert, R. Dittmann, R. Waser, R. A. De Souza, *Nanoscale* **2014**, *6*, 12864–12876.
[33] R. A. De Souza, *J. Mater. Chem. A* **2017**, *5*, 20334–20350.
[34] M. Gellert, K. I. Gries, C. Yada, F. Rosciano, K. Volz, B. Roling, *J. Phys. Chem. C* **2012**, *116*, 22675–22678.
[35] S. Kim, S. K. Kim, S. Khodorov, J. Maier, I. Lubomirsky, *Phys. Chem. Chem. Phys.* **2016**, *18*, 3023–3031.
[36] T. Bondevik, H. H. Ness, C. Bazioti, T. Norby, O. M. Lovvik, C. T. Koch, O. Prytz, *Phys. Chem. Chem. Phys.* **2018**, *21*, 17662–17672.
[37] S. K. Kim, S. Khodorov, C. T. Chen, S. Kim, I. Lubomirsky, *Phys. Chem. Chem. Phys.* **2013**, *15*, 8716–8721.
[38] C. S. Chang, I. Lubomirsky, S. Kim, *Phys. Chem. Chem. Phys.* **2018**, *20*, 8719–8723.

[39] X. Tong, D. S. Mebane, R. A. De Souza, *J. Am. Ceram. Soc.* **2019**, *103*, 5–22.
[40] H. Shiiba, N. Zettsu, M. Yamashita, H. Onodera, R. Jalem, M. Nakayama, K. Teshima, *J. Phys. Chem. C* **2018**, *122*, 21755–21762.
[41] S. Yu, D. J. Siegel, *Chem. Mater.* **2017**, *29*, 9639–9647.
[42] J. A. Dawson, P. Canepa, M. J. Clarke, T. Famprikis, D. Ghosh, M. S. Islam, *Chem. Mater.* **2019**, *31*, 5296–5304.
[43] H. Mehrer, *Diffusion in Solids*, Springer Verlag, Berlin Heidelberg New York, **2007**.
[44] S. Beschnitt, T. Zacherle, R. A. De Souza, *J. Phys. Chem. C* **2015**, *119*, 27307–27315.
[45] D. A. Andersson, S. I. Simak, N. V. Skorodumova, I. A. Abrikosov, B. Johansson, *Proc. Natl. Acad. Sci. USA* **2006**, *103*, 3518–3521.
[46] M. Nakayama, M. Martin, *Phys. Chem. Chem. Phys.* **2009**, *11*, 3241–3249.
[47] B. Grope, T. Zacherle, M. Nakayama, M. Martin, *Solid State Ionics* **2012**, *225*, 476–483.
[48] S. Grieshammer, B. O. H. Grope, J. Koettgen, M. Martin, *Phys. Chem. Chem. Phys.* **2014**, *16*, 9974–9986.
[49] P. P. Dholabhai, J. B. Adams, P. Crozier, R. Sharma, *J. Chem. Phys.* **2010**, *132*, 094104-1–8.
[50] R. A. De Souza, V. Metlenko, D. Park, T. E. Weirich, *Phys. Rev. B* **2012**, *85*, 174109.
[51] T. Zacherle, A. Schriever, R. A. De Souza, M. Martin, *Phys. Rev. B* **2013**, *87*, 134104-1–11.
[52] A. R. Genreith-Schriever, P. Hebbeker, J. Hinterberg, T. Zacherle, R. A. De Souza, *J. Phys. Chem. C* **2015**, *119*, 28269–28275.
[53] A. R. Genreith-Schriever, R. A. De Souza, *Phys. Rev. B* **2016**, *94*, 224304.
[54] T. G. Stratton, H. L. Tuller, *J. Chem. Soc. Faraday Trans. 2* **1987**, *83*, 1143–1156.
[55] H. L. Tuller, A. S. Nowick, *J. Electrochem. Soc.* **1979**, *126*, 209–217.
[56] J. Faber, C. Geoffroy, A. Roux, A. Sylvestre, P. Abelard, *Appl. Phys. A* **1989**, *49*, 225–232.
[57] K. Fuda, K. Kishio, S. Yamachi, K. Fueki, *J. Phys. Chem. Solids* **1985**, *46*, 1141–1146.
[58] S. B. Adler, J. W. Smith, J. A. Reimer, *J. Chem. Phys.* **1993**, *98*, 7613–7620.
[59] P. Vonlanthen, B. Grobety, *Ceram. Int.* **2008**, *34*, 1459–1472.
[60] E. C. Dickey, X. D. Fan, S. J. Pennycook, *J. Am. Ceram. Soc.* **2001**, *84*, 1361–1368.
[61] G. Arora, D. S. Aidhy, *J. Mater. Chem. A* **2017**, *5*, 4026–4035.
[62] D. S. Aidhy, Y. W. Zhang, W. J. Weber, *J. Mater. Chem. A* **2014**, *2*, 1704–1709.
[63] J. A. Purton, N. L. Allan, D. S. Gunn, *Solid State Ionics* **2017**, *299*, 32–37.
[64] A. R. Symington, M. Molinari, J. Statham, J. Wu, S. C. Parker, *J. Phys. Energy* **2019**, *1*, 042005.
[65] H. J. Heelweg, R. A. De Souza, A. R. Genreith-Schriever, *unpublished*.
[66] H. B. Lee, F. B. Prinz, W. Cai, *Acta Mater.* **2013**, *61*, 3872–3887.
[67] P. P. Dholabhai, J. A. Aguiar, L. J. Wu, T. G. Holesinger, T. Aoki, R. H. R. Castro, B. P. Uberuaga, *Phys. Chem. Chem. Phys.* **2015**, *17*, 15375–15385.
[68] P. V. Nerikar, K. Rudman, T. G. Desai, D. Byler, C. Unal, K. J. McClellan, S. R. Phillpot, S. B. Sinnott, P. Peralta, B. P. Uberuaga, C. R. Stanek, *J. Am. Ceram. Soc.* **2011**, *94*, 1893–1900.
[69] C. A. J. Fisher, H. Matsubara, *Solid State Ionics* **1998**, *113*, 311–318.
[70] Z. G. Mao, S. B. Sinnott, E. C. Dickey, *J. Am. Ceram. Soc.* **2002**, *85*, 1594–1600.
[71] M. Yoshiya, T. Oyama, *J. Mater. Sci.* **2011**, *46*, 4176–4190.
[72] A. Stukowski, *Model. Simul. Mat. Sci. Eng.* **2010**, *18*, 015012.
[73] E. J. W. Verwey, *Physica* **1935**, *2*, 1059–1063.
[74] N. F. Mott, R. W. Gurney, *Electronic Processes in Ionic Crystals*, Oxford University Press, New York, **1940**.
[75] L. A. Hughes, M. Marple, K. van Benthem, *Appl. Phys. Lett.* **2018**, *113*, 041604.
[76] M. Kunow, A. Heuer, *J. Chem. Phys.* **2006**, *124*, 214703.
[77] P. C. McIntyre, *J. Am. Ceram. Soc.* **2000**, *83*, 1129–1136.
[78] A. Tschoepe, C. Bauerle, R. Birringer, *J. Appl. Phys.* **2004**, *95*, 1203–1210.
[79] J. P. Parras, C. Cao, Z. Ma, R. Mücke, L. Jin, R. Dunin-Borkowski, O. Guillon, R. A. De Souza, *J. Am. Ceram. Soc.* **2020**, *103*, 1755–1764.
[80] A. Tschoepe, S. Kilassonia, R. Birringer, *Solid State Ionics* **2004**, *173*, 57–61.
[81] M. Born, J. E. Mayer, *Z. Phys.* **1932**, *75*, 1–18.
[82] G. Balducci, J. Kaspar, P. Fornasiero, M. Graziani, M. S. Islam, J. D. Gale, *J. Phys. Chem. B* **1997**, *101*, 1750–1753.
[83] T. X. T. Sayle, S. C. Parker, D. C. Sayle, *Phys. Chem. Chem. Phys.* **2005**, *7*, 2936–2941.
[84] T. X. T. Sayle, S. C. Parker, D. C. Sayle, *J. Mater. Chem.* **2006**, *16*, 1067–1081.
[85] T. X. T. Sayle, S. C. Parker, D. C. Sayle, *Faraday Discuss.* **2007**, *134*, 377–397.
[86] S. Plimpton, *J. Comput. Phys.* **1995**, *117*, 1–19.
[87] M. Wojdyr, S. Khalil, Y. Liu, I. Szlufarska, *Modelling Simul. Mater. Sci. Eng.* **2010**, *18*, 075009.
[88] P. V. Nerikar, D. C. Parfitt, L. A. C. Trujillo, D. A. Andersson, C. Unal, S. B. Sinnott, R. W. Grimes, B. P. Uberuaga, C. R. Stanek, *Phys. Rev. B* **2011**, *84*, 174105.

Manuscript received: June 5, 2020
Revised manuscript received: July 24, 2020
Accepted manuscript online: August 5, 2020

COMMUNICATIONS

Interfacial forces: The resistance arising from the perturbed crystal structure at a grain boundary of an inorganic oxide-ion conductor was determined by means of classical Molecular Dynamics simulations. Comparisons are made between this intrinsic structural resistance and resistances stemming from depletion space-charge layers.

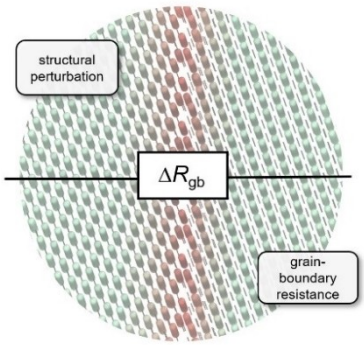

Dr. A. R. Genreith-Schriever, J. P. Parras, H. J. Heelweg, Prof. Dr. R. A. De Souza*